A tuning fork based wide range mechanical characterization tool with nanorobotic manipulators inside a scanning electron microscope

Juan Camilo Acosta,[1,a),c)] Gilgueng Hwang,[1,b),c)] Jérôme Polesel-Maris,[2] and Stéphane Régnier[1]

[1]*Institut des Systèmes Intelligents et de Robotique Université Pierre et Marie Curie, CNRS UMR 7222 4 Place Jussieu, 75252 Paris Cedex, France*

[2]*CEA, IRAMIS, Service de Physique et Chimie des Surfaces et Interfaces, F-91191 Gif-sur-Yvette, France*

(Received 12 August 2010; accepted 22 December 2010; published online 18 March 2011)

This study proposes a tuning fork probe based nanomanipulation robotic system for mechanical characterization of ultraflexible nanostructures under scanning electron microscope. The force gradient is measured via the frequency modulation of a quartz tuning fork and two nanomanipulators are used for manipulation of the nanostructures. Two techniques are proposed for attaching the nanostructure to the tip of the tuning fork probe. The first technique involves gluing the nanostructure for full range characterization whereas the second technique uses van der Waals and electrostatic forces in order to avoid destroying the nanostructure. Helical nanobelts (HNB) are proposed for the demonstration of the setup. The nonlinear stiffness behavior of HNBs during their full range tensile studies is clearly revealed for the first time. Using the first technique, this was between 0.009 N/m for rest position and 0.297 N/m before breaking of the HNB with a resolution of 0.0031 N/m. For the second experiment, this was between 0.014 N/m for rest position and 0.378 N/m before detaching of the HNB with a resolution of 0.0006 N/m. This shows the wide range sensing of the system for potential applications in mechanical property characterization of ultraflexible nanostructures. © *2011 American Institute of Physics*. [doi:10.1063/1.3541776]

I. INTRODUCTION

Recently, many ultraflexible and elastic micro/nanostructures have been synthesized as building blocks to create microelectromechanical systems/nanoelectromechanical systems (MEMS/NEMS).[1,2] Carbon nanotubes (CNTs),[3–6] Nanowires (NWs),[7] and nanohelixes[8–13] are the most widely synthesized and are considered as the promising elements for various NEMS and nanoelectronics. However, these devices are principally limited to laboratory prototypes, and so, they have not yet been commercialized. This is mainly due to the manufacturing challenges and physical properties which remain little known. For both of these problems, precise knowledge of the mechanical properties of these nanostructures is imperative. For example, the precise mechanical properties of NWs and NTs can predict their device characteristics. It also contributes to their arrayed growth and assembly in controlled direction thus, the manufacture of devices such as field emitters can be achieved.

The mechanical properties of these one-dimensional (1D) nanostructures could be studied using conventional atomic force microscopy (AFM) thanks to their simple mechanics. However, recently fabricated three-dimensional (3D) nanostructures such as 3D nanohelixes face their challenges to understand the complex mechanics. The 3D nanohelixes are inspired by nature and its complex mechanical properties. For example, the mechanics of 3D biological structures in nature such as deoxyribonucleic acid (DNA), proteins, cells, or tissues are complicated and being studied.[14] As inorganic nanohelixes, the electrical and mechanical properties of SiGe/Si/Cr and SiGe/Si Helical nanobelts (HNBs) were recently characterized separately through experiments and simulations.[12] The fabrication and mechanical characterization of InGaAs/GaAs HNBs have been also described.[13] Their excellent flexibility provides new avenues for fabrication of ultrasmall force sensors with high resolution as depicted in Fig. 1(a). The displacement of these nanohelixes was detected by a recently developed visual recognition[15] or piezoresistive smart sensing mechanism.[16] However, their mechanical properties were only studied in the limited upper displacement region mainly due to the lack of proper calibration tools for a full range mechanics study.[12,13] A high resolution and long range mechanical calibration system is, therefore, necessary.

As conventional force calibration tools, AFM,[17] piezoresistive cantilever,[18] capacitive force sensor,[19] and other MEMS (Ref. 20) have mostly been used. However, their sensing resolution and range are also limited as depicted in Fig. 1(b). This means that they are insufficient to characterize the full range of nanostructure mechanics.

For this reason, we need large range force sensing tools. Our approach uses tuning forks for wide range force sensing. They have been widely used in the watch industry. Recently, they have also been used as force sensors, mainly for imaging and manipulating matter under a scanning probe microscope,[21–23] and to function as force sensors inside SEM thanks to their simple readout system by replacing laser optics.[24] However, these last approaches were mainly limited to the integration of AFM imaging resolution in addition

a)Electronic mail: acosta@isir.upmc.fr.
b)Electronic mail: hwang@isir.upmc.fr.
c)These authors contributed equally to this work.

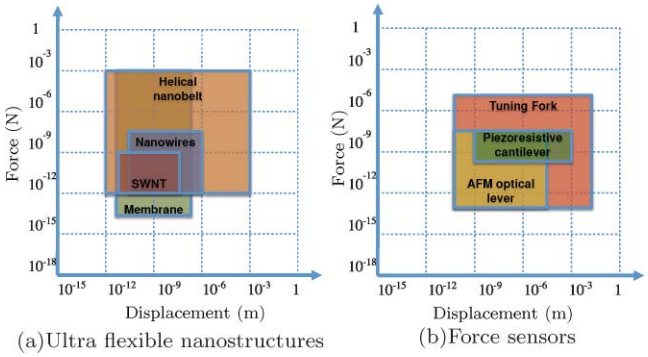

FIG. 1. (Color online) Force vs displacement diagram.

to the SEM imaging. Nanomanipulation systems based on tuning forks for mechanical characterization inside SEM have not yet been attempted.

To achieve this objective, we aim to develop a 3D nanomechanical property characterization system with large range and high resolution force sensing. The 3D characterization based on the developed sensor is achieved by SEM for an accurate visual detection and a nanomanipulation system with 3 degrees of freedom and nanometer positioning resolution. We propose a tuning fork based force sensor with a large range and a high resolution. The performance of the proposed system is proved by a full range tensile elongation study of HNB.

II. PRINCIPLES OF FORCE GRADIENT MEASUREMENT WITH A TUNING FORK

A. Overview of dynamic force sensing

Force measurement with a tuning fork is possible with standard AFM dynamic force sensing techniques, such as amplitude/phase modulation (AM/PM) and frequency modulation (FM) [see Table I]. For the first, a lock-in amplifier can be used in order to separate amplitude and phase from the original signal. From these two signals, the force can be obtained through an analytical conversion formula.[25,26] For the second, an automated gain controller (AGC) and a phase locked loop (PLL) controller are used to obtain the resonant frequency of the tuning fork. With the shift of the resonant frequency, the gradient of the force can be obtained.[27,28]

Selecting AM or FM depends mainly on the required settling time τ of the tuning fork. For AM–AFM regulation, the reaction time $\tau = Q/(\pi f_0)$ (where f_0 is the resonant frequency and Q is the quality factor) is highly dependent on the quality factor. Furthermore, the quality factor is higher in vacuum conditions of the SEM, and consequently, the bandwidth analysis will be limited. The FM–AFM removes the time constant dependency[29] of the analysis, thus allowing wide bandwidth with a high quality factor. This, therefore, makes it the primary selection for this work.

TABLE I. Amplitude modulation vs frequency modulation.

	AM/PM	FM
Electronic sensing	Amplitude (V)/Phase($^\circ$)	Frequency shift (Δf)
→ Physics sensing	Force	Force gradient
Settling time	$\tau = Q/(\pi f_0)$	$\tau \approx 1/f_0$

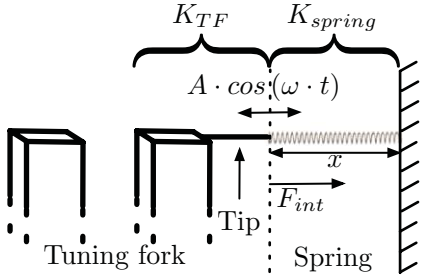

FIG. 2. Tuning fork mechanical model with virtual spring.

B. Frequency modulation gradient force sensing

The tuning fork frequency shift can be expressed as[30]

$$\frac{\Delta f}{f_0} = \frac{1}{A \cdot K_{\mathrm{TF}}} \int_0^{1/f_0} F_{\mathrm{int}}(\omega \cdot t) \cdot \cos(\omega \cdot t)\, dt, \qquad (1)$$

where K_{TF} is the stiffness of the tuning fork, A is the tuning fork mechanical oscillation amplitude, F_{int} is the interaction force between the tip of the tuning fork and the sample, f_0 is the resonant frequency of the tuning fork, Δf is the frequency shift, and ω is the angular frequency of the tuning fork.

A frequency shift implies a change in the force gradient. The object in contact is consequently deforming and can be modeled as a spring [Fig. 2]. The interaction force can then be modeled with Hooke's law [Eq. (2)], where K_{spring} represents the nonconstant stiffness of the object and Δx the deformation of the object.

$$F_{\mathrm{int}} = K_{\mathrm{spring}} \cdot \Delta x. \qquad (2)$$

The tip of the tuning fork is in contact, and aligned, with one end of the spring [Fig. 2]. Because of this alignment, the lateral stiffness of the tuning fork tip is not taken into account. Furthermore, the longitudinal stiffness of the tip is higher by several orders of magnitude than the spring, and so, can also be ignored. The elongation of the spring can be expressed as

$$\Delta x = A \cdot \cos(\omega \cdot t) + \delta x, \qquad (3)$$

where $A \cdot \cos(\omega \cdot t)$ is the contribution from the oscillation amplitude of the tuning fork probe, $f = \omega/(2 \cdot \pi)$, and δx is the linear elongation of the spring.

The interaction force F_{int} of the spring model [Eq. (2)] and the displacement Δx [Eq. (3)], can be replaced in the frequency shift of the tuning fork [Eq. (1)] resulting in Eq. (4), where the stiffness of the object modeled as a spring can be obtained in terms of the resonant frequency of the tuning fork, the frequency shift, and the stiffness of the tuning fork. Details on error estimation are collated in the Appendix,

$$K_{\mathrm{spring}} = \frac{2 \cdot \Delta f \cdot K_{\mathrm{TF}}}{f_0}. \qquad (4)$$

The stiffness of the tuning fork can be obtained using a geometrical model. The tuning fork dimensions can be measured, either with a microscope or SEM, thus the use of a geometrical method is feasible,

$$K_{\mathrm{TF}} = \frac{E \cdot w \cdot t^3}{4 \cdot l_1^3}. \tag{5}$$

In Eq. (5), w, t, and l_1 are the width, height, and length of the tuning fork prong (geometrical parameters of the tuning fork can be seen in Fig. 5) and $E = 78.7\,\mathrm{GPa}$, is the Young modulus of the quartz crystal of tuning forks. The stiffness of the tuning fork can be assumed constant.[23]

As A, K_{TF}, and f_0 are constant, Eq. (4) clearly shows that the measured frequency shift will reveal the stiffness behavior of the object.

III. TUNING FORK MECHANICAL CHARACTERIZATION SYSTEM

A. System overview

An *in situ* SEM tuning fork mechanical property characterization system is presented. An OC4-Station from SPECS-Nanonis is used for the oscillation control of the tuning fork and data acquisition. The advantages of this station are namely that it has a lock-in amplifier, a PLL, an AGC, a data acquisition hardware and software, and a real time operating system. The electronic preamplifier for the tuning fork was specially designed for use in SEM imaging conditions. These electronics will be fully described in a forthcoming article. A TT*i* EX752M multimode power supply unit was used with fixed ±5 V for the tuning fork electronic preamplifier. The detailed experimental setup is shown in Fig. 3. The main advantage of this system is that all the electronics for the tuning fork and the manipulators are outside the SEM chamber, thus avoiding any influences from the electron beam and space occupation.

For vacuum environment and visual feedback, a SEM (Leica stereoscan 260 cambridge instruments) is used. Two nanomanipulators (MM3A-EM and Kleindiek) are used to manipulate the nanostructures. Further details on the role of the manipulators and the manipulation procedure are described in Sec. IV. Each nanomanipulator has 3 degrees of freedom and, respectively, 5, 3.5, and 0.25 nm resolution at the tip in X, Y, and Z axis. Each axis is actuated with piezo stick-slip principle and is controlled via an open loop piezo controller. Configuration of the manipulators and the tuning fork inside the SEM chamber can be seen in Fig. 4.

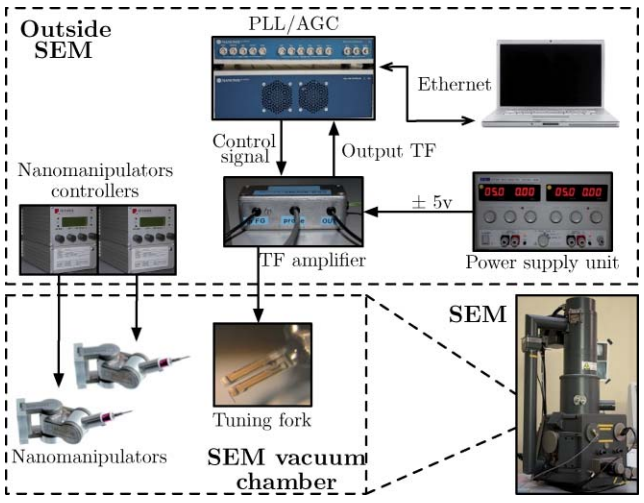

FIG. 3. (Color online) System configuration of used hardware inside and outside the SEM.

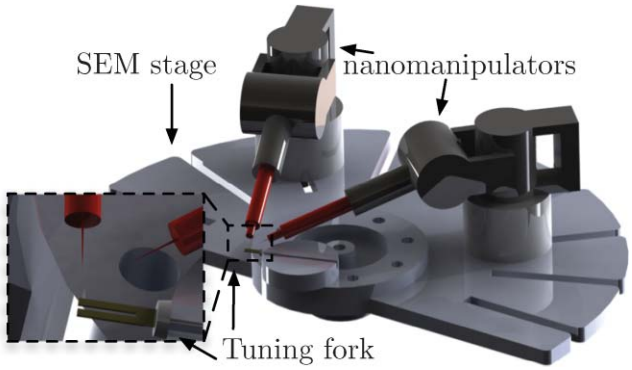

FIG. 4. (Color online) 3D CAD model of experimental setup of nanomanipulators and tuning fork inside SEM chamber.

The tuning forks were manufactured by Citizen America – CFS206 32.768KDZB-UB. A tip is attached to the tuning fork in order to fix it to the nanostructure. Picoprobes, tungsten tips (T-4-10-1 mm, tip radius: 100 nm, GGB industries), and tips made with platinum iridium Pt90/ir10 wires are used for the nanomanipulator and the tuning fork, respectively.

B. Tuning fork probe preparation

Several factors have to be considered before adding the tip. The quality factor of the tuning fork should remain as high as possible in order to obtain the highest sensitivity. It is based on balancing the weight between the two prongs. Any weight added to one of the prongs should be compensated by the other one so as to avoid decreasing the quality factor.[23] As shown in Fig. 5, for grounding with the prong of the tuning fork, electrically conductive silver epoxy EPO-TEK H21D (Epoxy Technology) is used to fix the tip, thus avoiding electrostatic charging by electron beam inside the SEM. Glue also needs to be added for weight compensation on the other prong of the tuning fork; this can be done with either conductive or nonconductive glue. As the electron beam is mainly focused

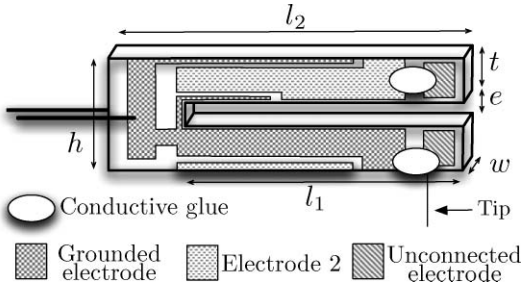

FIG. 5. Schematic of tuning fork electrodes with glued probe.

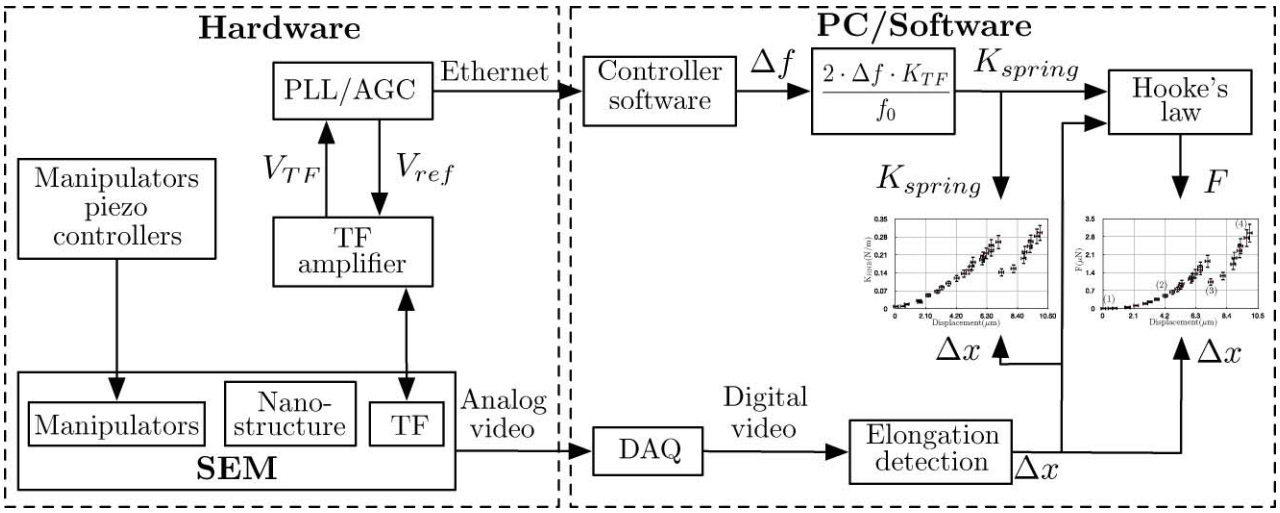

FIG. 6. Experiments' data flow for plot generation. The tuning fork frequency shift obtained, thanks to the PLL and AGC turned on, is then transformed to stiffness with Eq. (5), which is transformed to force with Hooke's law. SEM video feedback is imported to a computer with a data acquisition card. The elongation of the nanostructure is measured from video acquisition.

and zoomed on the tip of the probe, the other prong of the tuning fork has little risk of charging.

C. Data flow

The data flow of the entire experiment can be divided into three different and independent blocks (Fig. 6). The first is the nanomanipulator block. It is composed of both manipulators and their respective controllers for the piezoactuators. They are manually operated and are not connected to the rest of the setup. The second block represents all the hardware and software used for the tuning fork. The PLL and amplitude controller are needed to obtain the frequency shift. This frequency is acquired with LABVIEW based acquisition software and after the experiment is finished, it is transformed into the stiffness (under the assumption of the constant stiffness of the tuning fork[23]) and the constraint force of the measured object with Eqs. (4) and (2). The last block represents the SEM based visual feedback. Analog video signal from the SEM is imported with a data acquisition card and recorded. Once the experiment is finished, the visual detection is used to estimate the nanostructure elongation. Hence, the elongation measurement and the stiffness estimation of the nanostructure give the applied force of the nanostructure.

IV. MANIPULATION PROTOCOL

A. Assembly of nanostructure with manipulation setup

The tuning fork probe was fixed to the top of the SEM stage to avoid mechanical disturbances. In order to pick up the nanostructure, the free end of the nanostructure is attached to the tip of the manipulator. For this purpose, the probe of the manipulator is dipped into Nanopoxy glue [Fig. 7(a)], then it is brought closer to make contact with the end of the nanostructure [Fig. 7(b)]. The SEM electron beam is focused onto the glue to solidify it.

Two different attachments to the tip of the tuning fork and the nanostructure can be made. The first technique involves fixing the nanostructure with glue to the tip of the tuning fork. For this, glue is added to the tip of the tuning fork with the second nanomanipulator [Fig. 8(a)]. The nanostructure is then brought closer to nanomanipulator 1 to make contact with the tip of the tuning fork. The SEM electron beam is used to solidify the glue [Fig. 8(b)]. This technique allows full range characterization of the nanostructure, however, the nanostructure has to be destroyed eventually in order to disconnect the system. For the second experiment, electrostatic and van der Waals forces are used to maintain the nanostructure attached to the probe of the tuning fork. This is basically the same

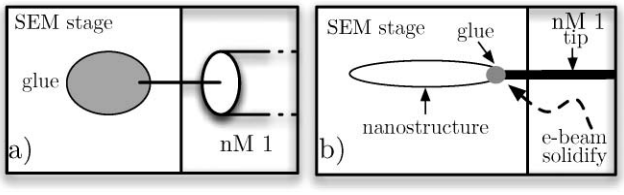

FIG. 7. Protocol for picking the nanostructure with manipulator tip. (a) Adding glue to the probe of the nanomanipulator. (b) Picking nanostructure from subtract with the nanomanipulator probe and soldering with e-beam. nM stands for nanomanipulator.

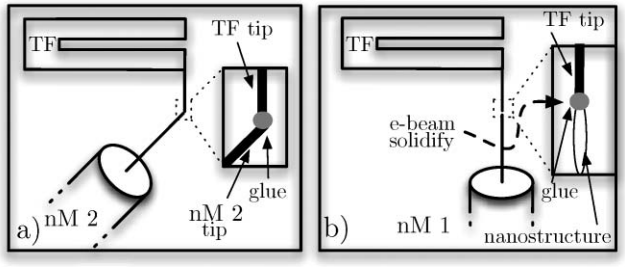

FIG. 8. Attachment with glue of the nanostructure to the tuning fork tip. (a) Adding glue to tip end of the tuning fork probe. (b) Attaching the nanostructure to the tuning fork tip and soldering with the electron beam.

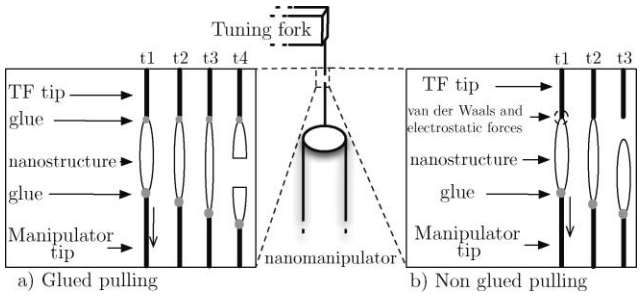

FIG. 9. Experimental protocol and configurations for longitudinal pulling. (a) Nanostructure glued to the tip of tuning fork. (b) Nanostructure not glued to the tip of tuning fork.

configuration except for the absence of applying chemical glue between the tuning fork probe and the nanostructure. Also, it is a nondestructive technique and can be repeated several times.

B. Experimental protocol

Usually, the lateral stiffnesses of ultraflexible nanostructures such as CNTs and HNBs are smaller than longitudinal ones by at least 1 order of magnitude. As a result, compressing the structure is very challenging; it might bend instead of compress. For this reason, the experimental protocol is focused on elongation of the nanostructure.

For the attachment with glue [Fig. 9(a)], the bond with glue is stronger than the mechanical resistance of the nanostructure. This guarantees that the nanostructure will break before the glue, and so full range characterization, can be achieved. For the second type of elongation [Fig. 9(b)], adhesion forces are used to maintain the bond between the nanostructure and the tip of the tuning fork. This bond depends mainly on the electrostatic force and depending on the dimensions and conductivity of the nanostructure, it could be higher or lower. Furthermore, this force can be increased by the SEM electron beam voltage and focusing it on the structure. At certain points during the elongation, the structure can be detached and the experiment can be repeated again.

V. HELICAL NANOBELT CHARACTERIZATION

InGaAs/GaAs bilayer HNBs were used for the experiments. The HNBs were fabricated by the process described in Ref. 16. Finite element method (FEM) simulation is used to estimate the deflection by the applied force onto HNBs, thus, obtaining the rest (at no elongation) stiffness. Longitudinal stiffness is estimated to be 0.009 N/m for HNB 1 and 0.011 N/m for HNB 2 as summarized in Table II. This simulation demonstrates the rest position stiffness of the HNB. Nevertheless, nonconstant behavior of the stiffness for upper elongation range was demonstrated by previous experimental works[13] with an AFM cantilever under SEM. However, in previous works, full range measurement was not attempted due to the lack of wide range force sensing.

Two tuning fork probes were used for the experiments. The geometry information and the estimated stiffness of the two tuning forks are summarized in Table III.

A. Full range mechanical characterization of HNB

For this experiment, the HNB 1 was attached between the tuning fork tip and the manipulator tip with glue for full range characterization. With the method described in Sec. III C, frequency shift [Fig. 10(a)], the elongation of the HNB [Fig. 10(b)], the HNB stiffness [Fig. 10(c)], and the constraint force of the HNB [Fig. 10(d)] were obtained. The frequency shift noise (estimated at 5 mHz) is much lower than the frequency shift steps due to the elongation of the HNB. As the manipulators have no position feedback, the displacements are estimated from the SEM recorded video at 33 Hz frame rate with a resolution of 0.2 μm for each measurement. Details on error estimation for frequency shift and force are summarized in the Appendix.

During the motion of the nanomanipulator, different geometrical configurations of the HNB stand out: these are compiled in Fig. 10(e). At the beginning of the experiment, the HNB is in rest position and the pitch looks homogeneous [Fig. 10(e)(1)]. The stiffness of the HNB for this position was obtained with finite element simulation. To obtain the experimental stiffness of the HNB for the rest position, the difference between the tuning fork resonant frequency before and after the HNB attachment to the tuning fork tip needs to be obtained. However, one of the main problems for this measurement was that the vacuum condition of the SEM improved over time, thus making the resonant frequency increase continuously. The order of magnitude of the frequency shift due to this is in a similar range to the frequency shift due to HNB attachment. As a result, the initial stiffness could not be measured and so, it was estimated by FEM. It should be noted that the initial stiffness model by FEM was confirmed by experiments.[13]

With elongation [Fig. 10(e)(2)], the HNB shows a nonhomogeneous pitch. This is due to the rotation constraint imposed by attaching glue to both sides. Further elongation increases the pitch differences in the HNB until one part of the

TABLE II. HNB specifications.

	HNB 1	HNB 2
Thickness of InGaAs/GaAs (nm)	11.6/15.6	11.6/15.6
Length (μm)	25.4	53.4
Pitch (μm)	3.9	8.9
Number of turns	6.5	6
Stripe width (μm)	1.5	2.5
Diameter (μm)	2	2.5
Longitudinal stiffness (FEM)(N/m)	0.009	0.011

TABLE III. Tuning forks' specifications with glued tip at the end of the prong.

	TF 1	TF 2
Resonant frequency f_0(Hz)	28325.5	30895.2
Stiffness k_{TF}(N/m)	7936	7936
Quality factor	11 145	19 800
Prong length l_1(μm)	3204	3204
Prong height t(μm)	382	382
Prong width w(μm)	238	238

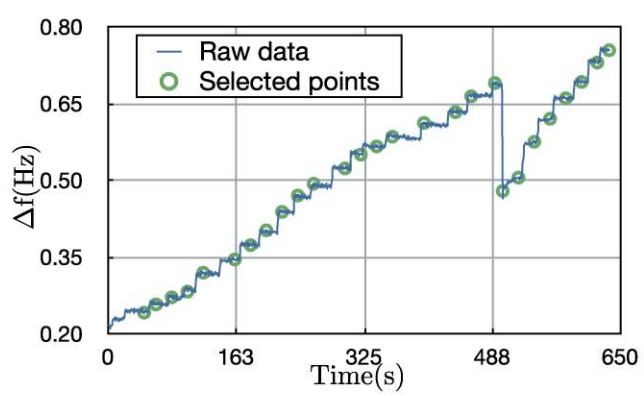

(a)Frequency shift from PLL and amplitude controller

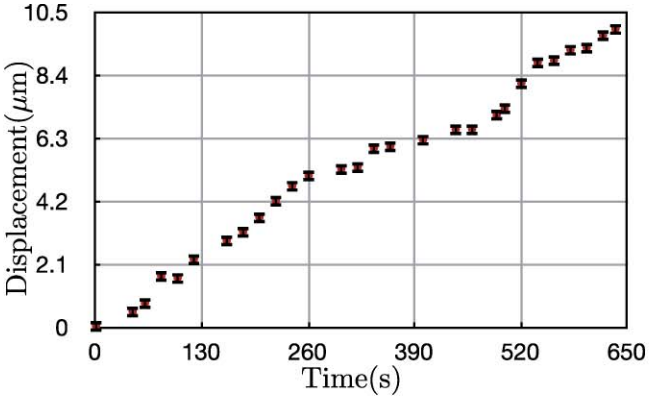

(b)Displacement from SEM visual feedback

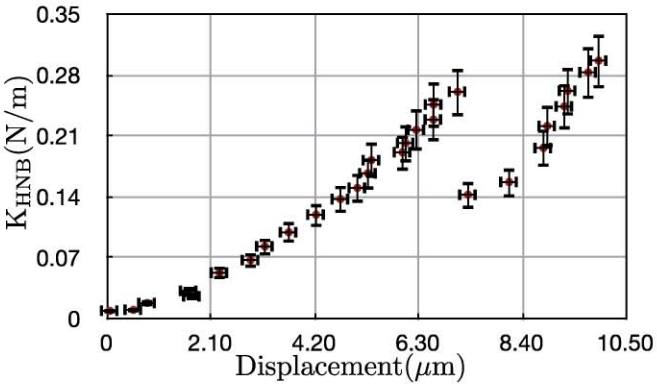

(c)HNB longitudinal stiffness

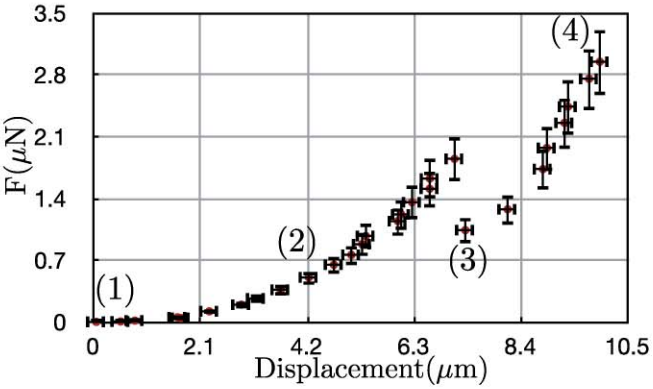

(d)Force.

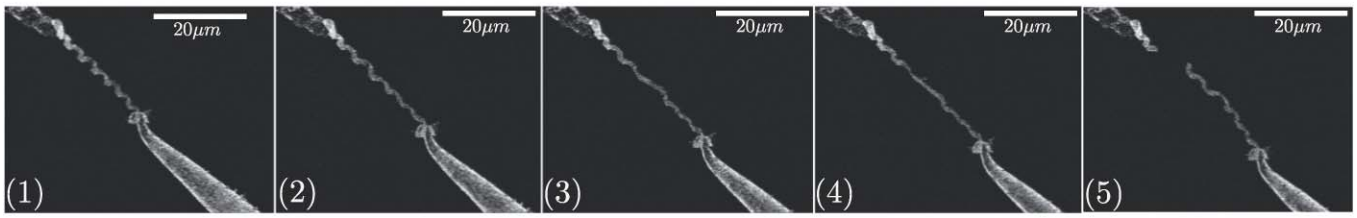

(e)Captures from SEM video. (1) HNB prior to pulling, (2) HNB during pulling, (3) HNB unrolling, (4) HNB before break, (5) HNB after break

FIG. 10. (Color online) Full range longitudinal pulling.

HNB unrolls at 7.3 μm displacement at 500 s [Fig. 10(e)(3)]. Subsequently, there is a release of the strain in the HNB that is reflected in a drop of the frequency shift, stiffness, and force [Figs. 10(a), 10(c), and 10(d)]. At this point, one section of the HNB is unrolled and damaged.

Finally, the HNB is elongated until it is almost completely unrolled and damaged just before breaking [Fig. 10(e)(4)]. The HNB then breaks [Fig. 10(e)(5)]. The contact between the tips and the HNB remains after breaking to ensure the attachment process.

These results confirm the nonconstant stiffness behavior of HNBs in full range elongation. In previous works,[13] where AFM cantilevers were inside the SEM, this behavior was not clearly measured for displacement of less than 10 μm. Furthermore, the nonhomogeneous pitch of this HNB has been revealed with the nonlinear behavior of the stiffness and SEM visual feedback. The resulting elongation force, therefore, shows a highly nonlinear behavior which goes from 14.5 nN for the smallest step made to 2.95 μN before breaking. This shows the wide range sensing of the system.

B. Nondestructive characterization

The previous experiment had three principal limitations, which we aim to solve in this second experiment. First, the vacuum conditions disturbed the resonant frequency of the tuning fork with an increasing offset as time went on. Second, it is a destructive method whereby the HNB is destroyed after the experiment, and the tips of the tuning fork and manipulator can become contaminated with glue and remaining parts of the HNB. In addition to this, attaching the HNB by both ends prevents its rotation during tensile elongation, and so eventually damaging it. Finally, the SEM video is manually analyzed. This means that for every frame of interest, the elongation of the HNB is estimated with manually placed points in the video.

In order to solve the first problem, vacuum characterization is done prior to the experiment to identify the saturation time after pumping where the variation of vacuum conditions will not affect the experiment. For this purpose, frequency shift is recorded during the pumping process [inset

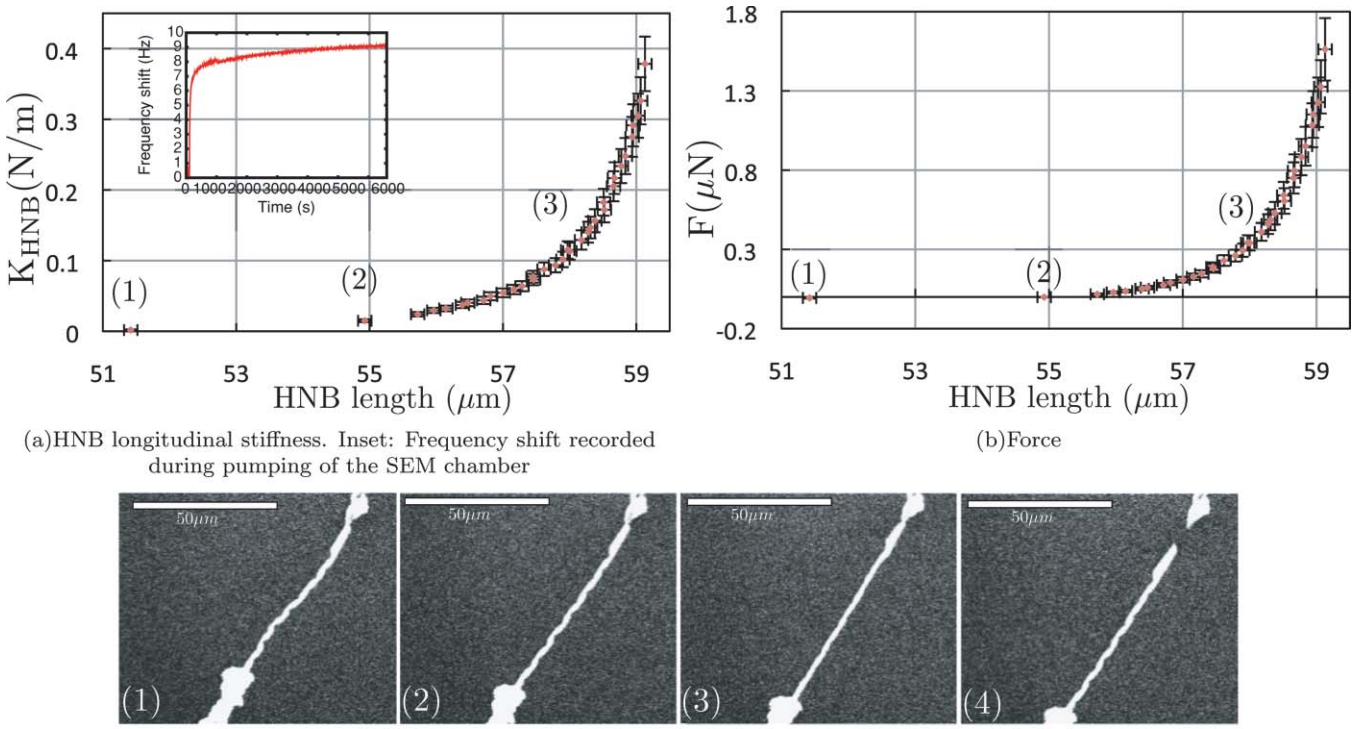

(a)HNB longitudinal stiffness. Inset: Frequency shift recorded during pumping of the SEM chamber

(b)Force

(c)Captures from SEM video. (1) HNB pushing (2) HNB rest elongation, (3) HNB pulling, (4) HNB after detachment.

FIG. 11. (Color online) Nondestructive longitudinal pulling.

Fig. 11(a)]. After 90 min, the frequency shift drift due to vacuum conditions is small enough for a 10 min experiment. To overcome the second problem, as explained in Sec. IV, electrostatic and van der Waals forces are used to maintain the HNB attached to the tip end of the tuning fork. Frequency shift noise decreased from 5 to 1 mHz due to the higher quality factor of the tuning fork. For the elongation of the HNB, offline visual tracking software[31] is used. This, in addition to the high contrast used in the SEM, makes the error decrease from 0.2 to 0.1 μm even though the scale passed from 20 to 50 μm.

The stiffness and force applied to the HNB are obtained in the same manner as previous experiments [Figs. 11(a) and 11(b)]. Four different moments of the experiment are highlighted. First [Fig. 11(c)(1)], the HNB is pushed and has a light "s-like" shape. This is mainly due to a much lower lateral stiffness than longitudinal stiffness of the HNB. Consequently, the stiffness measured is composed of both lateral and longitudinal and its absolute value is lower than the longitudinal rest position stiffness. The elongation, being negative, results in a negative force vector. After, the HNB is elongated to the rest position [Fig. 11(c)(2)]. and then, elongated further [Fig. 11(c)(3)] until it detaches from the probe of the tuning fork [Fig. 11(c)(4)].

In comparison to the previous experiment, a higher nonlinearity can be noticed. This is mainly due to the nonconstrained rotation of the end of the HNB in contact with the tuning fork. As a result, the HNB freely adjusts its number of turns through elongation, avoiding damages and the loss of a helical shape. Furthermore, the estimated force of 1.56 μN before releasing corresponds to the addition of van der Waals and electrostatic forces. The results of the experiments are detailed in Table IV.

TABLE IV. Summary of experiments results. Exp stands for experiment.

	Exp 1	Exp 2
Degrees of freedom of manipulator	3	
Manipulator resolution in *x*/*y*/*z* (nm)	5/3.5/0.25	
Frequency shift resolution (Hz)	0.005	0.001
→ Corresponding stiffness resolution (N/m)	0.0031	0.0006
HNB rest stiffness estimated by FEM (N/m)	0.009	0.011
HNB measured rest stiffness (N/m)	NA	0.014
HNB highest measured stiffness (N/m)	0.297	0.378
HNB highest measured elongation (μm)	9.95	4.13
→ Breaking/detaching force (μN)	2.95	1.56

VI. CONCLUSIONS

In situ SEM robotic nanomanipulation system for dynamic mechanical characterization of ultraflexible nanostructures has been presented. A frequency modulated tuning fork is used for gradient force sensing and a method for nanostructure stiffness estimation through the frequency shift of the tuning fork was developed. For manipulation of the nanostructures, two nanomanipulators are used and an assembly protocol is developed. Two experiment protocols are proposed. For the first, the nanostructure is fixed between the tips of the tuning fork probe and manipulator for full range characterization. For the second, electrostatic and van der Waals forces are used to keep the structure attached to the tip of the tuning fork, which allows nondestructive and repeatable characterization to be done.

For the demonstration of the system, HNBs were used. The nonconstant stiffness behavior of HNBs during their controlled tensile elongation was clearly revealed in full range for the first time to the best of our knowledge. The obtained stiffness ranges from 0.009 to 0.297 N/m with a resolution of 0.0031 N/m during full elongation and 0.011 to 0.378 N/m with a resolution of 0.0006 N/m for the nondestructive method. It was transformed into full elongation tensile forces as high as 2.95 μN for the first experiment and 1.56 μN for the second. The revealed nonlinear behavior of the stiffness with SEM visual feedback shows the capability of the proposed system to understand the mechanical properties of the nanostructure due to geometry deformation. The use of a lower spring constant tuning fork probe can dramatically improve the resolution. Despite this, the main limit of the system is the resolution of SEM visual analysis. Furthermore, the nanomanipulator can be installed on top of a closed loop controlled xyz piezo nanostage to obtain the displacement with more accuracy and increase the dexterity and resolution of the system.

The proposed system will allow dynamic mechanical characterization of other ultraflexible nanostructures, such as nanowires, nanotubes, and graphene membranes, to be possible in the future. Moreover, the dynamic measurement in addition to the dexterity of the system makes it ideal for measuring the dynamic oscillation mode of membranes for optical micromirror applications. Furthermore, by incorporating environmental electron microscopes or fluorescence optics, flexible and elastic biological nanostructures such as DNA, proteins, cells, and tissues are also in the scope of this new system.

ACKNOWLEDGMENTS

We would like to thank the French Atomic Energy Commission (CEA) Fontenay aux Roses for the SEM and facilities, and the University of Tokyo for allowing us to use the two Kleindiek manipulators with their respective controllers. We thank Guy Blaise for his SEM expertise at INSTN of CEA Saclay. We also thank François Thoyer, Jacques Cousty, Christophe Lubin, and Laurent Pham Van for their fruitful discussions. This work has been supported by the French National Project NANOROL ANR-07-ROBO-0003.

APPENDIX: NANOSTRUCTURE STIFFNESS AND FORCE ERROR ESTIMATION

The nanostructure stiffness and force error are obtained with error propagation method in Eqs. (4) and (2).

$$
\begin{aligned}
&eK_{\text{spring}} \\
&= \left|\frac{\delta K_{\text{spring}}}{\delta K_{\text{TF}}}\right| \cdot eK_{\text{TF}} + \left|\frac{\delta K_{\text{spring}}}{\delta \Delta f}\right| \cdot e\Delta f + \left|\frac{\delta K_{\text{spring}}}{\delta f_0}\right| \cdot ef_0 \\
&= \frac{2}{f_0} \cdot \left(\Delta f \cdot eK_{\text{TF}} + K_{\text{TF}} \cdot e\Delta f + \frac{K_{\text{TF}} \cdot \Delta f \cdot ef_0}{f_0}\right),
\end{aligned}
\tag{A1}
$$

$$
\begin{aligned}
eF &= \left|\frac{\delta F}{\delta K_{\text{spring}}}\right| \cdot eK_{\text{spring}} + \left|\frac{\delta F}{\delta x}\right| \cdot ex \\
&= x \cdot eK_{\text{spring}} + K_{\text{spring}} \cdot ex,
\end{aligned}
\tag{A2}
$$

where eK_{TF}, $e\Delta f$, and ef_0 are the estimation error of the tuning fork stiffness, the frequency shift, and the resonant frequency. Here, ex is the spring elongation estimation error with SEM visual feedback.

[1] R. Saeidpourazar and N. Jalili, IEEE Trans. Ind. Electron. **55**, 3935 (2008).
[2] R. Smith, D. Sparks, D. Riley, and N. Najafi, IEEE Trans. Ind. Electron. **56**, 1066 (2009).
[3] H. Dai, J. H. Hafner, A. G. Rinzler, D. T. Colbert, and R. E. Smalley, Nature (London) **384**, 147 (1996).
[4] J. H. Hafner, C. Cheung, T. H. Oosterkamp, and C. M. Lieber, J. Phys. Chem. B **105**, 743 (2001).
[5] J. Li, A. M. Cassell, and H. Dai, Surf. Interface Anal. **28**, 8 (1999).
[6] S. Iijima, Nature (London) **354**, 56 (1991).
[7] Y. Cui and C. M. Lieber, Science **291**, 851 (2001).
[8] S. Motojima, M. Kawaguchi, K. Nozaki, and H. Iwanaga, Appl. Phys. Lett. **56**, 321 (1990).
[9] X. B. Zhang, X. F. Zhang, D. Bernaerts, G. van Tendeloo, S. Amelinckx, J. van Landuyt, V. Ivanov, J. B. Nagy, P. Lambin, and A. A. Lucas, Europhys. Lett. **27**, 141 (1994).
[10] X. Y. Kong and Z. L. Wang, Nano Lett. **3**, 1625 (2003).
[11] P. X. Gao, Y. Ding, W. Mai, W. L. Hughes, C. Lao, and Z. L. Wang, Science **309**, 1700 (2005).
[12] D. J. Bell, Y. Sun, L. Zhang, L. X. Dong, B. J. Nelson, and D. Grützmacher, "Three-dimensional nanosprings for electromechanical sensors," Sens. Actuators A: Physical **130–131**, 54 (2006).
[13] D. J. Bell, L. Dong, B. J. Nelson, M. Golling, L. Zhang, and D. Grützmacher, Nano Lett. **6**, 725 (2006b).
[14] V. Vogel and M. Sheetz, Nat. Rev. Mol. Cell Biol. **7**, 265 (2006).
[15] B. Kratochvil, L. Dong, L. Zhang, and B. Nelson, J. Microsc. **237**, 122 (2010).
[16] G. Hwang and H. Hashimoto, Nano Lett. **9**, 554 (2009).
[17] D. J. Müller, W. Baumeister, and A. Engel, Proc. Natl. Acad. Sci. U.S.A. **96**, 13170 (1999).
[18] S. Park, M. B. Goodman, and B. L. Pruitt, Proc. Natl. Acad. Sci. U.S.A. **104**, 17376 (2007).
[19] F. Beyeler, S. Muntwyler, and B. J. Nelson, J. Microelectromech. Syst. **18**, 433 (2009).
[20] Y. U. Sun and B. J. Nelson, J. Inf. Acquis. **1**, 23 (2004).
[21] K. Karrai and R. Grober, Appl. Phys. Lett. **66**, 1842 (1995).
[22] F. J. Giessibl, Appl. Phys. Lett. **76**, 1470 (2000).
[23] A. Castellanos-Gomez, N. Agraït, and G. Rubio-Bollinger, Nanotechnology **20**, 215502 (2009).
[24] M. Todorovic and S. Schultz, "Magnetic force microscopy using nonoptical piezoelectric quartz tuning fork detection design with applications to magnetic recording studies" J. Appl. Phys. **83**, 6229 (1998).
[25] A. J. Katan, M. H. van Es, and T. H. Oosterkamp, Nanotechnology **20**, 165703 (2009).
[26] S. Hu and A. Raman, Nanotechnology **19**, 375704 (2008).
[27] F. J. Giessibl, Phys. Rev. B **56**, 16010 (1997).
[28] J. E. Sader and S. P. Jarvis, Appl. Phys. Lett. **84**, 1801 (2004).
[29] T. R. Albrecht, P. Grutter, D. Horne, and D. Rugar, J. Appl. Phys. **69**, 668 (1991).
[30] J. E. Sader, T. Uchihashi, M. J. Higgins, A. Farrell, Y. Nakayama, and S. P. Jarvis, Nanotechnology **16**, S94 (2005).
[31] "Kinovea - motion tuner," http://www.kinovea.org.